Electrochimica Acta 462 (2023) 142689

Contents lists available at ScienceDirect

Electrochimica Acta

journal homepage: www.journals.elsevier.com/electrochimica-acta

Wells-Dawson type polyoxometalate, $[S_2W_{18}O_{62}]^{4-}$-doped poly (3,4-ethylenedioxythiophene) films: Voltammetric behaviour and applications to selective bromate detection

Indherjith Sakthinathan [a], Naoki Yamasaki [b], Davide Barreca [c], Chiara Maccato [c,d], Tadaharu Ueda [b,e,f], Tim McCormac [a,*]

[a] Electrochemistry Research Group, Department of Applied science, Dundalk Institute of Technology, Dublin Road, Dundalk, County Louth A91K584, Ireland
[b] Department of Marine Resource Science, Faculty of Agriculture and Marine Science, Kochi University, Nankoku 783-8502, Japan
[c] CNR-ICMATE and INSTM, Department of Chemical Sciences, Padova University, Padova 35131, Italy
[d] Department of Chemical Sciences, Padova University and INSTM, Padova 35131, Italy
[e] Marine Core Research Institute, Kochi University, Nankoku 783-8502, Japan
[f] MEDi center, Kochi University, Kochi 780-0842, Japan

A B S T R A C T

Wells-Dawson type polyoxometalate (POM) $[(n\text{-}C_3H_7)_4N]_4S_2W_{18}O_{62}$ (S_2W_{18}) was successfully immobilised with a conducting polymer, poly(3,4-ethylenedioxythiophene) (PEDOT), by chronocoulometry technique. The immobilised films with different surface thicknesses were characterised by various electrochemical techniques. The S_2W_{18}-doped PEDOT film gave four couples of redox waves, the first one corresponds to the redox process of the polymer itself and the other three couples are electron transfer at tungstate in the framework. The films exhibited inherent pH-dependent redox activity and stability of S_2W_{18} in the thin layer up to 100 mV/s. Only slight changes were observed in the magnitude of peak currents after continuous redox cycling, indicating the relative stability of the S_2W_{18} in the conducting PEDOT. The conductive behaviour of the film was investigated with electrochemical impedance spectroscopy. The study of electrochemical bromate ion sensing based on S_2W_{18}-doped PEDOT film employing chronoamperometric technique revealed that at an applied potential of -0.1 V, the S_2W_{18}-doped PEDOT film can detect bromate at concentrations between 100 μmol L^{-1} and 2000 μmol L^{-1}. Moreover, the S_2W_{18}-doped PEDOT film shows a detection limit of 4 μmol L^{-1} without interference from other common ions present in the water. Hybrid films exhibit significant catalytic activity with high selectivity at a low reduction potential of -0.1 V. Chemico-physical characterization of the target systems was performed using atomic force microscopy, field emission scanning electron microscopy, energy dispersive X-ray spectroscopy and Raman spectroscopy.

1. Introduction

Polyoxometalates (POMs) are a distinctive class of inorganic metal-oxo clusters consisting of high-valent transition metals (M) (e.g. M = V, Mo, W) which are linked through oxygens[1]. In recent decades, POMs are the prospective candidate for various applications such as electro-catalysis [2–4], photo-catalysis [5–7], sensors [8,9], electrochemical energy storage devices [10,11], electronics [12], and photoelectrochemical devices [13], owing to the unique electronic, optical, magnetism and redox properties related to their structural features. In most cases of the application of POMs, especially catalysts, immobilization of them is required to use heterogeneously because they are anion and soluble in media. Many researchers have studied different strategies to anchor the POM on various materials [14]. Deposition techniques, including layer-by-layer deposition [15,16], self-assembly monolayers [17,18], Langmuir–Blodgett [19,20], sol-gel films [21,22], electrodeposition [23,24], and entrapment into conducting polymers [25,26]. In addition, controlling the layer thickness, composition and orientation is an important criterion for establishing good electrical conductivity between the POM and the electrode surface. Electro-polymerised incorporation of POMs into the conducting polymer could provide efficient electrical communication with controlling layer thickness [1], which is one of the most promising techniques.

Among the many polymers: polyaniline, poly(3,4-ethylenedioxythiophene) (PEDOT), polypyrrole, polyacetylene, polythiophene, Poly(diphenylamine), Poly(p-phenylene), the PEDOT can serve better conductivity, stability, and high electrocatalytic activity [5,27]. Yuan *et al.* successfully fabricated a polyoxometalate (POM)-doped PEDOT hybrid film counter electrode, which was then used for the first time in dye-sensitized solar cells (DSSCs) [5]. McCormac and his

* Corresponding author.
E-mail addresses: tim.mccormac@dkit.ie, chuji@kochi-u.ac.jp (T. McCormac).

https://doi.org/10.1016/j.electacta.2023.142689
Received 25 January 2023; Received in revised form 4 May 2023; Accepted 31 May 2023
Available online 1 June 2023

research group have immobilised Kerb-type metal substituted POM into the PEDOT films and investigated the electrochemical and surface properties [26].

Extensive attention has been paid to the development of electrochemical determination methods of the trace amount of contaminants in water and food due to its rapidity, high sensitivity, excellent selectivity, and environmental friendliness compared to other techniques [28]. Bromate ion, BrO_3^-, is often found in drinkable water, because of ozonation and/or chlorination disinfection processes, as well as in flour and fish paste as a food additive [29,30]. Butler *et al.* reported a complete summary of the toxicity of BrO_3^- [31]. International Agency for Research on Cancer (IARC) has classified BrO_3^- as a potent cancer-inducing agent. Hence, high-performance electrochemically active materials must be acquired for sensitive and selective detection of bromate. Keggin and Wells-Dawson-type POMs have been widely used as electrocatalysts for the electrochemical detection of bromate due to their multiple redox behaviour [25]. In comparison to the Wells-Dawsons type POMs, Keggin-type POMs have been better researched for bromate detection. G. G. Papagiann and colleagues reported on the preparation and use of composite materials of polyaniline and Keggin-type POM as a bromate sensor [32]. Gold nanoparticles-stabilised PMo_{12}-doped-PEDOT were investigated as catalysts for electrochemical bromate detection by S. S. Hassan *et al* [33]. Two pyrazole derivatives, one symmetrical, namely 1,1-bis(3,5-dimethyl-1H-pyrazol-4-yl)methane, and one asymmetrical, namely 4-propyl-4,5-dihydro-1H-pyrazole, two polyoxometalates (POM)-based complexes constructed from saturated Wells–Dawson and mono-Cu (II)-substituted Keggin anions, respectively, were hydrothermally synthesized. The carbon paste electrodes of both of these were then used as electrochemical sensors to detect hydrogen peroxide, bromate, and nitrite [34]. However, most cases have issues in terms of selectivity at lower reduction potential.

In this paper, Wells-Dawson type POM, $[(n\text{-}C_3H_7)_4N]_4S_2W_{18}O_{62}$ (S_2W_{18}), has been successfully immobilised on the PEDOT polymer matrix using the chronocoulometry technique. The S_2W_{18}-doped PEDOT film showed four couples of redox waves which were stable towards potential cycling through several $W^{VI/V}$ redox states at different sites of S_2W_{18}. The films of various thicknesses were constructed. The modified electrode was performed as a good electrochemical bromate sensor with high selectivity among the other interfering analytes such as chlorate, nitrite, phosphate, iodate, perchlorate and nitrate.

2. Experimental section

2.1. Materials

3,4-Ethylenedioxythiophene (EDOT) was purchased from Sigma. All other chemicals and solvents were purchased as reagent grade from ACROS Organics. Polishing alumina powder of sizes 0.05, 0.3, and 1.0 μm was received from CH instruments. Highly purified water was obtained from a Milli-Q water purification system (ELGA PURELAB Option Q7) with a resistivity of 18.2 MΩ cm and was used throughout the preparation of an aqueous electrolyte solution. The following reagents were used to prepare the Buffer solution of various pH: 0.1 mol L^{-1} Na_2SO_4 (pH 2-3), 0.1 mol L^{-1} Na_2SO_4 + 20 mmol L^{-1} CH_3COOH (pH 3.5-5), 0.1 mol L^{-1} Na_2SO_4 + 20 mmol L^{-1} of $NaHPO_4$ (pH 5.5-7). The pH of the solution was finally adjusted with either 0.1 mol L^{-1} of H_2SO_4 or 0.1 mol L^{-1} of NaOH solution depending on the required pH.

2.1.1. Synthesis of $[(n\text{-}C_3H_7)_4N]_4S_2W_{18}O_{62}$

The $((n\text{-}C_3H_7)_4N)_4[S_2W_{18}O_{62}]$ was prepared based on the reported procedure with a minor modification [35]. To a 16.5 g solution of $Na_2WO_4{\cdot}2H_2O$ in 490 ml of water was added 400 mL of CH_3CN. Then, 110 mL of concentrated H_2SO_4 was added dropwise with vigorous stirring; suspension occurred upon the addition of a few drops of conc. H_2SO_4 and the next drops were added after the suspension had been cleared within several seconds. The solution was refluxed for one day. After the solution was cooled to room temperature, 300 mL of CH_3CN was added to produce two liquid layers. After the lower turbid layer was discarded, 10 g of *n*-Pr_4NBr was added to precipitate a yellow salt. The salt was collected by filtration, washed with water and ethanol, and air-dried to yield 7.5 g of the product, which was subsequently purified by recrystallization from 200 mL of CH_3CN at room temperature.

2.2. Instrumentation

All the electrochemical experiments reported in the article except electrochemical impedance were carried out using CHI-440a electrochemical workstation (USA) with a three-electrode electrochemical cell. Electrochemical impedance measurements were recorded in CHI-660 electrochemical workstation (USA). The glassy carbon electrode (GCE) with a geometric surface area of 0.0707 cm^2 was used as the working electrode; a platinum wire with a diameter of 0.5 mm and a length of 5 cm as the counter electrode and Ag/AgCl (saturated KCl) as the reference electrode. In the case of cyclic voltammetry in organic solvents and chronocoulometry Ag/Ag^+ was used as the reference electrode. The potential was transferred to Fc/Fc^+ (Fc=ferrocene) scale in a cyclic voltammogram in DMSO.

Atomic force microscopy (AFM) analyses were carried out using a NT-MDT SPM Solver P47H-PRO apparatus operating in tapping mode, using NSG03 probes [material: single-crystal Si, n-type; chip size: 3.4 mm x 1.6 mm x 0.3 mm; reflective side: Au; guaranteed tip curvature radius: 10 nm; cantilever length: (135±5) mm; cantilever width: (30±3) mm; cantilever thickness: (1.5±0.5) mm; typical resonant frequency: 90 kH; typical force constant: 1.74 N/m]. Micrographs recorded on different sample areas enabled to confirm surface homogeneity. After background subtraction and plane fitting, root-mean-square (RMS) roughness values were obtained from 3×3 μm^2 images according to the following relation:

$$\mathrm{RMS-roughness} = \left[\sum (z_i - Z)^2 \Big/ n\right]^{1/2} \quad (1)$$

where z_i, Z and n are the local height, the mean height and the number of data points, respectively.

Field emission-scanning electron microscopy (FE-SEM) and energy dispersive X-ray spectroscopy (EDXS) analyses were performed on a Zeiss SUPRA 40VP microscope equipped with an INCA x-act PentaFET Precision spectrometer (Oxford Instruments), operating at primary beam acceleration voltages between 10 and 20 kV and using in-lens and secondary electron detectors. The ImageJ® software [http://imagej.nih.gov/ij/, accessed December, 2022] was used for image analysis aimed at the estimation of the average aggregate dimensions. Raman spectroscopy measurements were carried out on a Labram HR instrument (Horiba) with a 50x (0.55 N.A) long-distance magnification objective (Leica). The laser source excitation wavelength was 785 nm (laser power = 10 %). The instrument was calibrated using a Si(100) wafer calibrated to its standard peak at 520.7 cm^{-1} and the Rayleigh line before the measurement of the sample [36].

2.3. Preparation of working electrode

A solution of 0.1 mol L^{-1} of monomer EDOT and 5 mmol L^{-1} of POM in acetonitrile were taken in the electrochemical cell and a constant potential of +0.85 V *vs* Ag/Ag^+ was applied to prepare the hybrid film with the various thickness by applying various deposition charges (1, 2, 5, and 10 mC) over the GCE leading to various thickness of the composite. After the hybrid film was deposited on the electrode surface, it was rinsed with acetonitrile to remove the unbounded solution. Finally, the electrode was washed with a buffer solution in which the film was used to study. The PEDOT-only film was formed by using the same procedure with the presence of 0.01 mol L^{-1} tetrabutylammonium

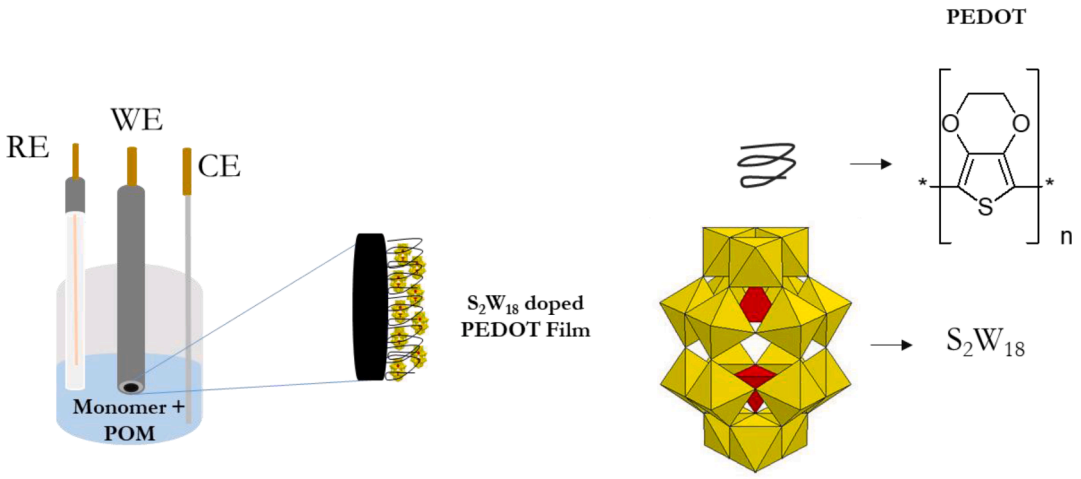

Fig. 1. Pictorial representation of S_2W_{18}-doped PEDOT film on the glassy carbon electrode.

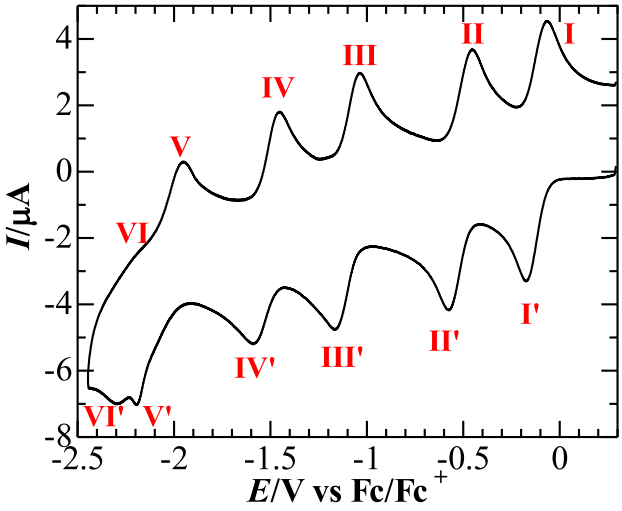

Fig. 2. Representative cyclic voltammogram of $[S_2W_{18}O_{62}]^{4-}$ in DMSO (0.1 mol L^{-1} *n*-Bu_4NPF_6). Scan rate: 100 mV/s.

hexafluorophosphate (*n*-Bu_4NPF_6) in acetonitrile.

S_2W_{18}-doped PEDOT (2 mC and 10 mC) films were deposited on the surface of ITO-coated glass plates using the same procedure to investigate the system morphology.

2.4. Electrochemical impedance spectroscopy (EIS)

Electrochemical impedance spectroscopy measurements were carried out using a CHI 660 electrochemical instrument with S_2W_{18}-doped PEDOT-modified electrode. The recording of the spectra was performed at different applied potentials (*vs.* Ag/AgCl) from 0.01 to 1 × 10^5 Hz with a voltage amplitude of 5 mV. Impedance spectra were analysed by fitting equivalent electrical circuits using electrochemical impedance spectrum analyser software [25].

Fig. 1

3. Results and discussion

3.1. Electrochemical behaviour of $[(n\text{-}C_3H_7)_4N]_4S_2W_{18}O_{62}$

A cyclic voltammogram was measured in the dimethyl sulfoxide containing 0.5 mmol L^{-1} of S_2W_{18} and 0.1 mol L^{-1} *n*-Bu_4NPF_6 as the supporting electrolyte at the surface of the GC working electrode at a scan rate of 100 mV/s (Fig. 2).

Table 1
Electrochemical data of $[S_2W_{18}O_{62}]^{n-}$ (n=4-10) in DMSO.

Compound	Peak	E_m (V *vs* Fc/Fc^+)	ΔE_p (mV)
$S_2W^{VI}_{18}/S_2W^{V}W^{VI}_{17}$	I	-0.13	115
$S_2W^{V}W^{VI}_{17}/S_2W^{V}_{2}W^{VI}_{16}$	II	-0.52	130
$S_2W^{V}_{2}W^{VI}_{16}/S_2W^{V}_{3}W^{VI}_{15}$	III	-1.11	130
$S_2W^{V}_{3}W^{VI}_{15}/S_2W^{V}_{4}W^{VI}_{14}$	IV	-1.53	140
$S_2W^{V}_{4}W^{VI}_{14}/S_2W^{V}_{5}W^{VI}_{13}$	V	-2.08	240
$S_2W^{V}_{5}W^{VI}_{13}/S_2W^{V}_{6}W^{VI}_{12}$	VI	-2.23	150

The six redox peaks that appeared in the voltammogram are associated with the tungsten-oxo species present in the Dawson structure [37,38]. These six peaks are correlated with the literature and each of the peaks represents a single electron transfer and a total of six electron transfers [38]. The peaks labelled, as I to VI are the mono electronic redox couples with E_m(E_m=(E_{pc}+E_{pa})/2, where E_{pc} and E_{pa} are cathodic and anodic peak potentials, respectively) and peak-separation, ΔEp (=E_{pa} - E_{pc}), values given in Table 1. All the processes are diffusion-controlled since the current magnitude for each peak is dependent on the square root of the used scan rates [39]. This voltammetric behaviour of the S_2W_{18} is explained in equations 2 to 7 [37,40].

$$\left[S_2W^{VI}_{18}O_{62}\right]^{4-} + e^- \leftrightarrow \left[S_2W^{V}W^{VI}_{17}O_{62}\right]^{5-} \quad (2)$$

$$\left[S_2W^{V}W^{VI}_{17}O_{62}\right]^{5-} + e^- \leftrightarrow \left[S_2W^{V}_{2}W^{VI}_{16}O_{62}\right]^{6-} \quad (3)$$

$$\left[S_2W^{V}_{2}W^{VI}_{16}O_{62}\right]^{6-} + e^- \leftrightarrow \left[S_2W^{V}_{3}W^{VI}_{15}O_{62}\right]^{7-} \quad (4)$$

$$\left[S_2W^{V}_{3}W^{VI}_{15}O_{62}\right]^{7-} + e^- \leftrightarrow \left[S_2W^{V}_{4}W^{VI}_{14}O_{62}\right]^{8-} \quad (5)$$

$$\left[S_2W^{V}_{4}W^{VI}_{14}O_{62}\right]^{8-} + e^- \leftrightarrow \left[S_2W^{V}_{5}W^{VI}_{13}O_{62}\right]^{9-} \quad (6)$$

$$\left[S_2W^{V}_{5}W^{VI}_{13}O_{62}\right]^{9-} + e^- \leftrightarrow \left[S_2W^{V}_{6}W^{VI}_{12}O_{62}\right]^{10-} \quad (7)$$

3.2. Electrochemical behaviour of $[S_2W_{18}O_{62}]^{4-}$- doped PEDOT film

The S_2W_{18}-doped PEDOT film was fabricated on the surface of the GC working electrode employing the above-mentioned procedure (*vide supra*). PEDOT is formed through the *in-situ* oxidative polymerisation of EDOT at the applied potential of 0.85 V vs Ag/Ag^+. PEDOT acquires positive charges during the oxidation processes, which must be stabilised by counterions, in this case, anionic POMs. POMs enter the polymer

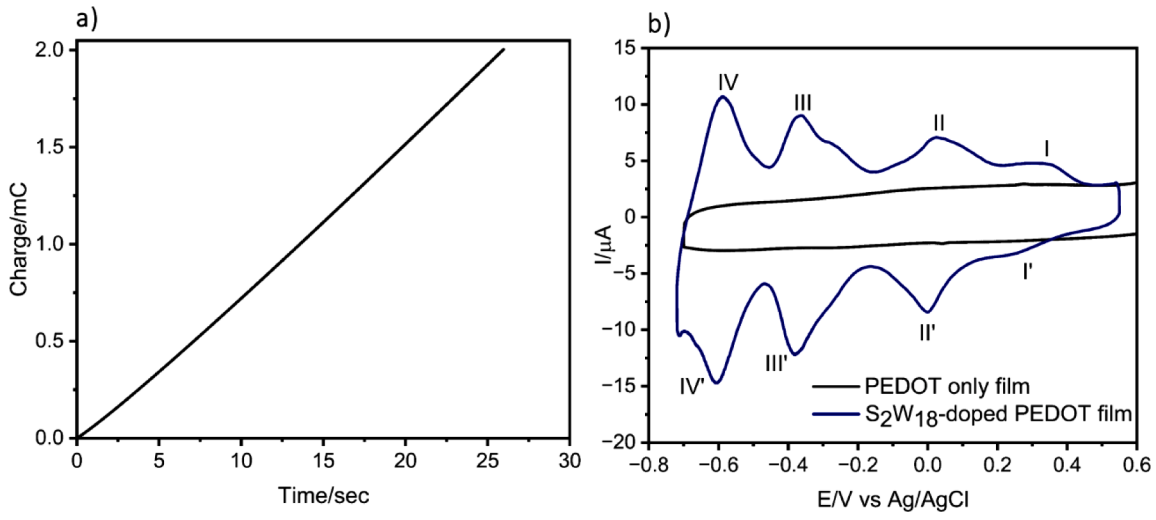

Fig. 3. a) Chronocoulometry polymerisation of S_2W_{18}-doped PEDOT film. b) A cyclic voltammogram of S_2W_{18}-doped PEDOT film (2 mC) (surface coverage of 1.72 nmol cm^{-2}) on GC electrode surface in pH 2 buffer solution. Scan rate: 10 mV/s.

matrix to stabilize the charge on the polymer backbone, resulting in the formation of the POM/PEDOT complex [41–43]. Fig. 3a shows the formation of S_2W_{18}-doped PEDOT film using the chronocoulometry technique. The electrochemical behaviour of the modified electrode was then investigated in a buffer solution at pH 2.

The formation of the S_2W_{18}-doped PEDOT film was confirmed by comparing the electrochemical behaviour of the hybrid film with the solution electrochemistry of the S_2W_{18}. Fig. 3b shows the redox electrochemistry of the resulting 2 mC hybrid layer recorded in pH 2 buffer at the scan rate of 10 mV/s. The cyclic voltammogram shows four distinct peaks labelled as I/I', II/II', III/III', and IV/IV'. The peak I/I' at E_m= 0.306 V corresponds to the redox process of the polymer matrix itself which was matched with the previously reported literature [44, 45]. The precise mechanism underlying the electrochemical conversion of PEDOT and polythiophene derivatives is not well understood [46]. However, according to Skompska [47,48] and Hillman *et al.* [49] the PEDOT polymer film has two different types of regions that coexist. They have reported two oxidation potentials, one for the oxidation of highly ordered short conjugated chains, and the most anodic potentials for the oxidation of less ordered short conjugated chains [46,50]. Each of the other three well-defined peaks at E_m= 0.012 V, -0.372 V, and -0.596 V corresponded to the redox behaviour of $W^{VI/V}$ in the framework of S_2W_{18} with the ΔE_p values of 24 mV, 17 mV, and 16 mV, respectively. Amna Yaqub *et al.* reported three POM-based well-defined redox processes for the $[S_2W_{18}O_{62}]^{4-}$doped polypyrrole film at half-wave potentials of -0.06, -0.43, and -0.66 V (vs Ag/AgCl). The S_2W_{18}-doped PEDOT film's E_m values are fairly close to the values that have been published [51]. The shifting of reversible potentials for the Wells-Dawson POM toward positive when the presence of water was reported by Bernardini *et al.* [37]. The two-electron transfer processes occur at each redox peak potential in the S_2W_{18}-doped PEDOT film, as shown in equations 8-10. Similar behaviour was previously reported in the Wells-Dawson type $[P_2Mo_{18}O_{62}]^{4-}$ [52].

$$\left[S_2W_{18}^{VI}O_{62}\right]^{4-} + 2e^- + 2H^+ \rightleftharpoons \left[H_2S_2W_2^{V}W_{16}^{VI}O_{62}\right]^{4-} \quad (8)$$

$$\left[H_2S_2W_2^{V}W_{16}^{VI}O_{62}\right]^{4-} + 2e^- + 2H^+ \rightleftharpoons \left[H_4S_2W_4^{V}W_{14}^{VI}O_{62}\right]^{4-} \quad (9)$$

$$\left[H_4S_2W_4^{V}W_{14}^{VI}O_{62}\right]^{4-} + 2e^- + 2H^+ \rightleftharpoons \left[H_6S_2W_6^{V}W_{12}^{VI}O_{62}\right]^{4-} \quad (10)$$

The role of the polymer was to stabilize the POM over the surface of the electrode. The distinctive feature of conducting polymer was observed from the increase in non-faradaic current and the presence

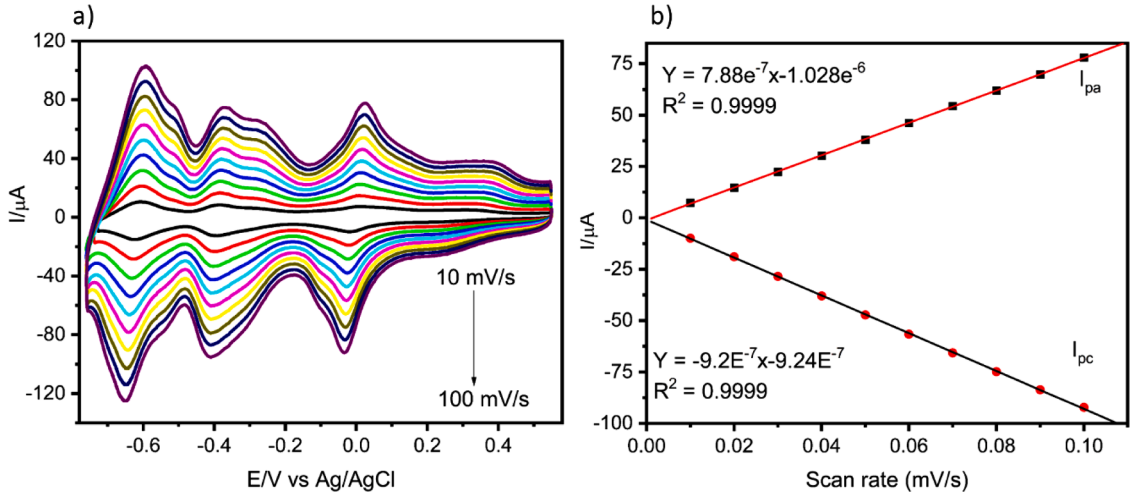

Fig. 4. a) Cyclic voltammograms of S_2W_{18}-doped PEDOT film (2 mC) measured at various scan rates in pH 2 buffer solution and b) relationship between scan rate and the magnitude of cathodic and anodic peak current at the II/II' process.

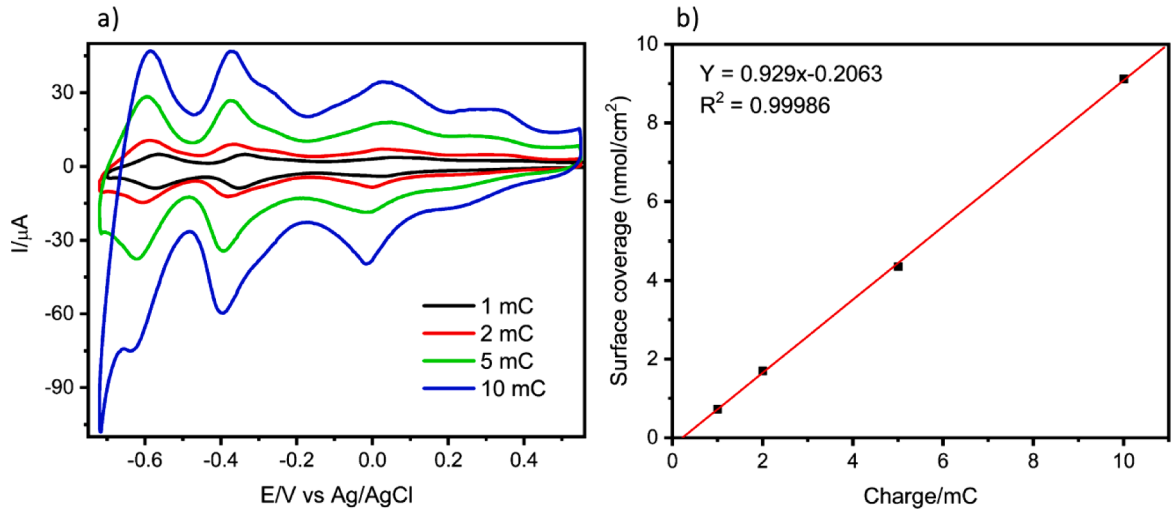

Fig. 5. a) Cyclic voltammograms of S_2W_{18}-doped PEDOT film of various surface thicknesses in pH 2 buffer solution. Scan rate: 10 mV/s. (b) Relationship between surface coverage of S_2W_{18}-doped PEDOT film and deposition charge.

faradaic peak (Peak I/I') in the positive region of the voltammogram [25]. The polymer contribution to the electrochemical response of the S_2W_{18}-doped film is relatively low; the voltammetric behaviour shown in Fig. 3b was dominated by the POM redox properties. However, the peak II/II' was broadened due to the polymer peak I/I'. Fig. 3b also contains the cyclic voltammogram of the fabricated 2 mC PEDOT-only film without the POM using the same experimental setup. Interestingly, the CV behaviour of PEDOT without the POM showed no redox peak corresponding to the polymer backbone. As previously reported, the electrochemical and physical properties of polymers are greatly influenced by the nature of the dopant and electrolyte during the polymerization process [49,53]. The pH study provides additional confirmation that the redox peak I correspond to the polymer's backbone (*vide infra*).

The surface coverage of the immobilized POM in the PEDOT polymer matrix was calculated at a slow scan rate by using equation (11).

$$\Gamma = Q/nFA \tag{11}$$

Where Γ (mol/cm^2) is the surface coverage for the surface-confined active species, Q (Coulomb) is the charge passed associated with a particular redox process, n is the number of electrons transferred, A is the surface area of the electrode in cm^2 and F is the Faraday constant (96,485 C/mol) [25,26].

The surface coverage of S_2W_{18}-doped PEDOT film with a deposition charge of 1 mC, 2 mC, 5 mC, and 10 mC for Γ_{ox} associated with the redox couple III/III′ was found to be 0.73, 1.7, 4.35, and 9.12 nmol cm^{-2} respectively. Noteworthy, the background non-faradaic current of the polymer was taken into account while calculating the charge. For example, to determine the charge (Q) of the S_2W_{18}-doped PEDOT 2 mC film, its corresponding polymer background was subtracted.

A scan rate study was carried out to find the surface-confined behaviour of the modified electrode. A hybrid film of a 2 mC deposition charge was used to record the scan rate effect in the pH 2 buffer (Fig. 4a). From Fig. 4b, we observe the increase in peak current with increasing the scan rate. The linear relationship between the current magnitude and scan rate was observed, indicating the surface-confined behaviour of the modified electrode [54]. In the case of scan rates higher than 100 mV/s, the electron transfer process of S_2W_{18} in the film was diffusion-controlled.

Fig. 5a shows the cyclic voltammograms of the S_2W_{18}-doped PEDOT film with various deposition charges (1-10 mC). As the deposition charge increases, the reduction of the polymer itself occurred at a more positive and the current magnitude increases in the reduction of doped S_2W_{18}, indicating peak broadening due to the inherent behaviour of the polymer (Charging current) and an increase in the concentration of S_2W_{18} doped, respectively. The linear relationship between the deposition charge and surface coverage was obtained from the plot of surface coverage (Γ) calculated using peak III anodic charges (Q) of *vs.* deposition charge (Fig. 5b).

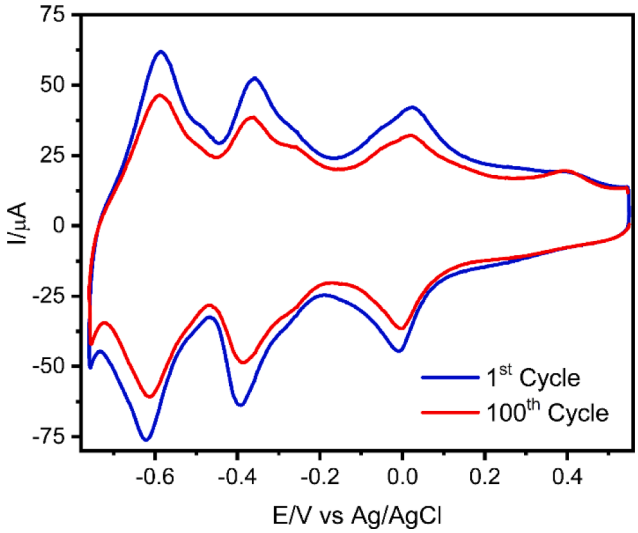

Fig. 6. Cyclic voltammograms of S_2W_{18}-doped PEDOT film (2 mC) at the 1st (Blue) and 100th (Red) potential cycle in pH 2.0 buffer solution. Scan rate: 100 mV/s.

To investigate the stability of the S_2W_{18}-doped PEDOT film, continuous cyclic voltammograms were measured in a potential range from +0.55 V to -0.8 V (Fig. 6). After 100 potential cycles, the peak current magnitude slightly decreased, indicating that the S_2W_{18}-doped film maintained its stability for multi-potential scanning.

The surface coverage at the 1st and 100th potential cycle was calculated from the cathodic charge of peak II and was found to be 1.72 and 1.56 nmol cm^{-2}, respectively, which indicated 90% of the hybrid film stuck on the surface of the electrode.

3.3. *Effect of pH*

Voltammetric behaviour of POMs highly depends on acid concentrations in both the solution and surface-confined state [54–58]. Cyclic

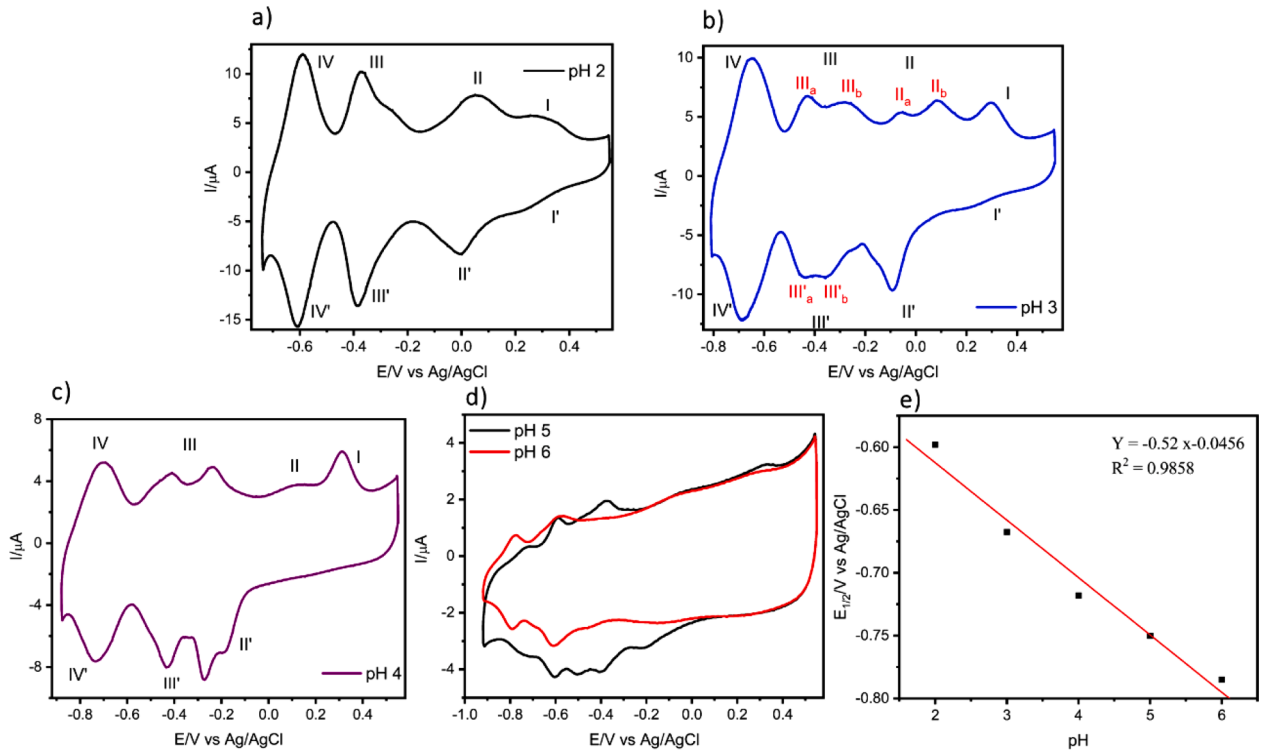

Fig. 7. Cyclic voltammograms of S_2W_{18}-doped PEDOT film (2 mC) in pH=a) 2, b) 3, c) 4, d) 5 and 6 buffer solution. Scan rate: 10 mV/s. e) The plot of pH *versus* redox half-wave potential of peak IV/IV' redox process.

voltammograms of S_2W_{18}-doped PEDOT (2 mC) film were measured at various pHs as shown in Fig. 7. As pH increases, the peak potential shift toward more negative with a decrease in the current magnitude. The hybrid film was stable up to pH 4, whereas it was unstable at pH > 5. Fig. 7b and c show the behaviour of hybrid film at pH 3 and 4 respectively. The bi-electronic nature of the peaks II/II' and III/III' can be seen in Fig. 7b and c. The bi-electronic oxidation peak (II) was split into two mono-electronic peaks in pH 3 which were labelled as IIa and IIb, which was very common in the Wells Dawson type polyoxometalates [59]. However, the splitting of the reduction peak (II') was not clear due to polymer interference. Similar behaviour was also observed with the redox peak III, in this case, both the reduction and oxidation peaks split into two mono-electronic each in pH 3. The peak I/I' was stable up to pH 4 and began to fade when the pH reached 5 because POM is not stable at those pHs that destabilise the polymer film. Furthermore, peak I/I' did not split like peaks II and III, confirming that peak I/I' corresponds to the polymer. A plot of pH vs $E_{1/2}$ values calculated for the peak IV/IV' shows the increment of $E_{1/2}$ values respective to the pH, which shows the peak corresponds to the redox behaviour of S_2W_{18} dependent on the pH of the solution (Fig. 7e).

3.4. Electrochemical impedance spectroscopy

EIS is used as a versatile technique to evaluate the interfacial and transport properties of the S_2W_{18}-doped polymer films [60,61]. The estimation of parameters such as diffusion coefficient and charge transfer resistance that explain the kinetics of the interface became relatively easy and accurate as compared to other techniques. Naseer *et al* studied the electrical properties of the Kerb-type transition metal-substituted POM-doped PEDOT film [26]. Di *et al* studied the interfacial properties of the Dawson-type vanodotungstophosphate and carbon nanotubes composite films [62].

The EIS was performed for the S_2W_{18}-doped PEDOT film to investigate the electrical properties using the Randle equivalent circuit. Two series of experiments were performed: first, measurements were carried

Fig. 8. Randle equivalent circuit [26] was used to measure impedance data performed at the GCE electrode modified with the S_2W_{18}-doped PEDOT films.

out in pH 2.0 buffer solution at five different potentials (0.2, 0.4, 0, -0.2, and -0.4 V vs Ag/AgCl) chosen to encompass the redox reactions of the S_2W_{18}. Secondly, measurements were carried out at four different thickness values at 0.0 V vs Ag/AgCl.

All spectra were fitted using the equivalent circuit shown in Fig. 8. In Fig. 8, R_s represents the uncompensated solution resistance between the electrolyte and electrode, Q_{dl} is the double-layer capacitance, which is here replaced by constant phase element (CPE), R_{ct} is the charge transfer resistance, and Z_w is the resistance by the diffusion of the electroactive species, also known as the Warburg impedance. Z_w is negligible at the higher frequency range with higher R_{ct} values being attained at such frequencies, indicating the kinetically controlled region, while at lower frequencies, Z_w is dominant, thereby indicating a diffusion-controlled process [27,63].

The films give lower R_{ct} values in the positive domain (+0.4 V) as compared to those when the film is further exposed to negative potential (-0.2 and -0.4 V), which are similar to the results previously observed in the literature [25,26]. The kinetically controlled region is not clear, while the diffusion-controlled region was observed with very lower R_{ct} values, indicating that the faster electron transfer should occur on the interface between S_2W_{18}-doped PEDOT film and solution at a particular applied potential (Fig. 9a). Table 2 summarizes the parameters such as solution resistance, charge transfer resistance, and complex impedance or Warburg impedance R_L, which arises by the diffusion of electroactive species for both reduced and oxidised domains of S_2W_{18}-doped PEDOT film.

Table 2 shows that the CPE values increased at both extreme

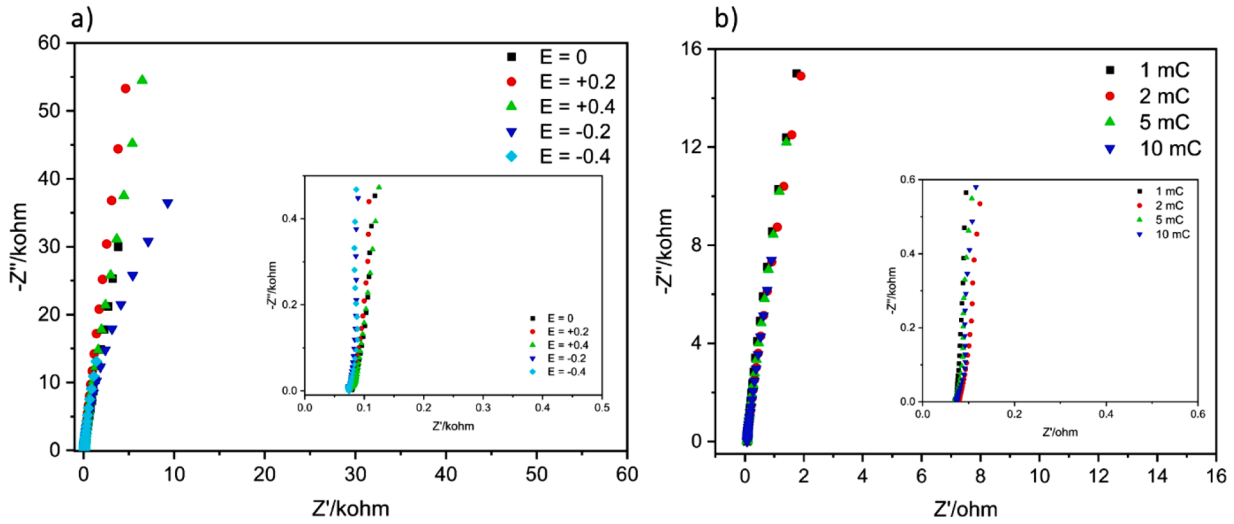

Fig. 9. a) Nyquist plots of S_2W_{18}-doped PEDOT film (2 mC) and the applied potentials were +0.0 V, +0.2 V, –0.2 V, +0.4 and –0.4 V in the pH 2.0 buffer (b) Nyquist plots of different thickness of S_2W_{18}-doped PEDOT film (formal potential 0.0 V) on GCE. The frequency range is between 0.01 to 10^5 Hz. The amplitude of the applied sine wave potential in each case was 5 mV. Insets: Zoomed images of the respective figure.

Table 2
Solution resistance R_i (Ω), charge transfer resistance R_{ct} (Ω), complex impedance R_L (Z_w), capacitance CPE (μF cm^{-2} $s^{\alpha=1}$), and exchange current density i_o (mA) were obtained from the A.C. impedance measurement of the S_2W_{18}-doped PEDOT film (2 mC) in pH 2 buffer solution.

E(V)	R_i (Ω)	R_{ct} (Ω)	R_L (Z_w)	CPE (μF cm^{-2} $s^{\alpha=1}$)
0.4	68	9.4	464	24
0.2	67	6.4	220	15
0	74	4.5	306	3
-0.2	51	11.6	17	8
-0.4	73	27	9	26

potential ranges and decreased at potentials that were near zero. The Warburg impedance was modelled as an open-circuit finite Warburg element that includes a diffusion resistance, R_{dif}. It is the resistance by the diffusion of the electroactive species (S_2W_{18}) from a modified probe to the analyte or vice versa. From the positive domain to the negative domain, the Warburg (Z_w) was decreased. The fact that the addition of PEDOT: POM makes the polymer film more electrolyte accessible is confirmed by the measured drop in Warburg impedance [64]. During the redox process there will be charge intercalation occurs at the conducting polymer to maintain the electro neutrality, in that case, Zw is replaced by CPE, known as low-frequency capacitance (Qlf). At lower frequencies, the capacitive behaviour is found and it can be related to the film charging mechanism [65]. The increase in CPE indicates that more ions are accommodated in the double layer at higher potentials, most likely due to the higher polarization material.

The electrochemical impedance behaviour of different S_2W_{18}-doped PEDOT film thicknesses was also recorded and shown in Fig. 9b. No significant difference was observed in the various thicknesses of the film.

3.5. Electrochemical bromate sensor

The S_2W_{18}-doped PEDOT film-modified GC electrode was employed to detect the bromate in the water and found that the S_2W_{18}-doped PEDOT film was potentially active toward the bromate ion. Cyclic voltammogram shows the S_2W_{18} and PEDOT hybrid film-modified GC electrode (2 mC) in pH 2 buffer in the absence and presence of bromate within the potential range of 0.55 V to -0.2 V (Fig. 10a). The reduction

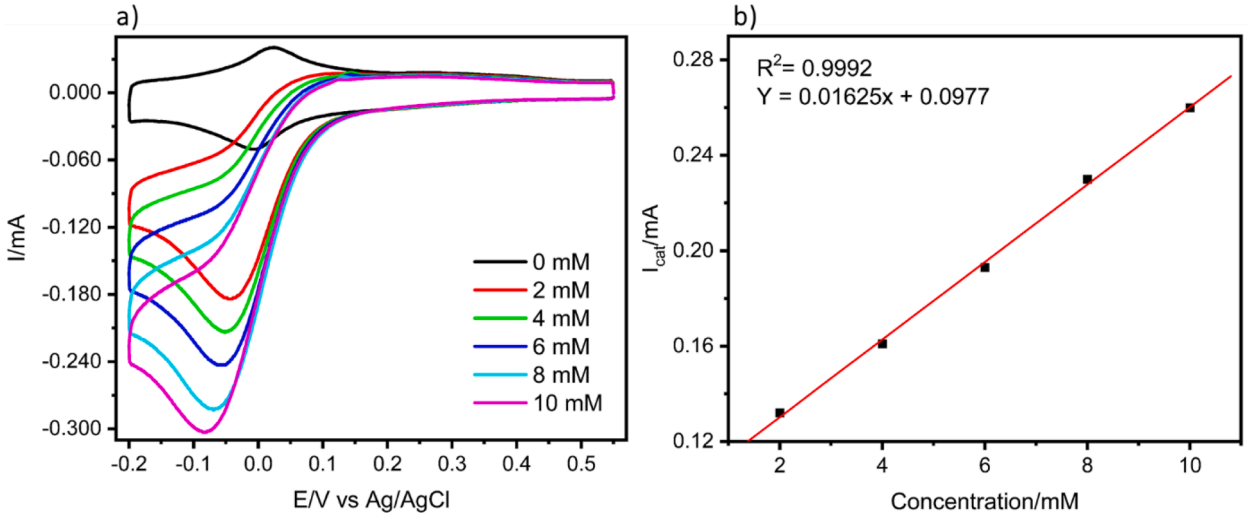

Fig. 10. a) Cyclic voltammograms of S_2W_{18}-doped PEDOT film (2 mC) in pH 2.0 at scan rate 50 mV/s in the presence of designated concentrations of bromate (0 - 10 mmol L^{-1}). b) Relationship between concentrations of bromate and current magnitude at peak II.

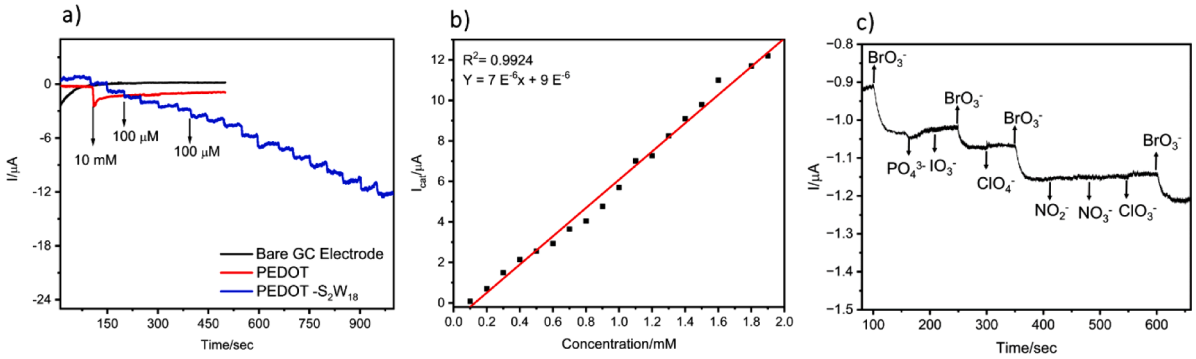

Fig. 11. a) Typical amperometric response of the bare GCE in comparison of a PEDOT and S_2W_{18}-doped film (2 mC) in pH 2.0 buffer at the applied potential of –0.1 V on successive addition of 100 μmol L^{-1} bromate up to 2 mmol L^{-1}. b) Relationship between concentrations of bromate and catalytic current. c) Response of the S_2W_{18}-doped PEDOT film towards the interference anions (1 mmol L^{-1}) and the bromate (100 μmol L^{-1}) at a polarization potential –0.1 V.

Table 3
Amperometry data for S_2W_{18}-doped PEDOT-based films of various thicknesses for catalysis of bromate in buffer pH 2.0.

Film (mC)	Sensitivity μAcm^{-2}/ mmol L^{-1}
1	42
2	97
5	45
10	30

current associated with peak II increases with increasing the concentration of the bromate ion. The relationship between the catalytic current response (I_{cat}) and bromate ion concentration is displayed in Fig. 10b. By subtracting the current response of the bromate ion at a given concentration from the current response of the S_2W_{18}-doped PEDOT 2 mC in the absence of any analyte, I_{cat} was calculated.

The amperometric response of the bare GCE toward the bromate ion (10 mM) demonstrates the catalytic inactivity of bare GC towards the bromate ion (Fig. 11a). The amperometric response of the PEDOT-alone modified electrode towards the bromate ion (10 mmol L^{-1}) shows no significant catalytic current, indicating the contribution of the conducting polymer does not greatly influence the catalytic reduction of bromate (Fig. 11a). On the other hand, the S_2W_{18}-doped PEDOT film (2 mC) gave a linear increase in current depending on the successive addition of bromate ion up to 2 mmol L^{-1} (Fig. 11a and b). The S_2W_{18}-doped PEDOT film of surface coverages in the range of 1.72 nmol cm^{-2} showed a sensitivity of 97.59 μAcm^{-2}/mmol L^{-1} with a limit of detection (LOD) of 4 μmol L^{-1} based on three times recorded S/N ratio. Moreover, the average time required to detect the bromate in the solution calculated from the amperometry technique was 3.46 sec.

The current response of the S_2W_{18}-doped PEDOT film as a bromate sensor was monitored in the presence of anions typically co-present in real samples such as $NaNO_3$, $NaNO_2$, KH_2PO_4, $NaIO_3$, $NaClO_4$ and $NaClO_3$ (1 mmol L^{-1}). The fact that the current-time response obtained for the successive addition of interference ion showed no interference at all indicates high selectivity of the S_2W_{18}-doped PEDOT film for the bromate detection (Fig. 11c). The electrocatalytic performance of the other thicknesses against the bromate ion has also been studied in order to determine the optimal layer for better electrocatalytic performance. Table 3 shows the variation in sensitivity of different thicknesses of the S_2W_{18}-doped PEDOT-based film with different surface coverage towards bromate.

The S_2W_{18}-doped PEDOT films of other thicknesses show significantly less sensitivity towards the bromate ion when compared to the 2 mC S_2W_{18}-doped PEDOT film. The large thickness of the polymer film, which prevents the diffusion of bromate ions through the polymer matrix to reach the active POM sites, may be the cause [66–68]. As a result, the electrocatalytic activity toward bromate decreases as the film thickness increases. EDOX analysis further confirmed the large contribution of polymer in the 10 mC film (*vide infra*). The loading of POM was insufficient in the case of the 1 mC film to obtain additional active sites for the reduction of bromate ions [69–71]. The film with a deposition charge of 2 mC showed the best catalytic performance.

To better understand the system and make further improvements, it has now become necessary to compare the catalytic performances of the S_2W_{18}-doped PEDOT, with the electrochemical bromate activity of the

Table 4
Comparison of the proposed sensor with reported literature.

Materials	Reduction potential (V vs Ag/AgCl)	Linear Range (μmol L^{-1})	Sensitivity μAcm^{-2}/ mmol L^{-1}	Detection limit (μmol L^{-1})	Ref
PMo_{12}/PEDOT/AuNP[a]/GC	0.142	250 - 3000	68	-	[33]
Polyaniline–POM	- 0.3	7.5 - 500	-	3	[32]
1–CPE[c] (P_2W_{18})	+ 0. 4	20 - 48	201.53	18	[34]
$[Ni_4(P_8W_{48}O_{184})(WO_2)]^{28-}$ POM+PPY[b] film	- 0.22	100 - 2000	4.91	0.2	[25]
$(H_{6/5}bppy)^{5-}$ $[P_2W_{18}O_{62}]\cdot 4.5H_2O$	-0.4	-	-	-	[73]
1-GCE $H_{1.73}P_2As_{1.73}W_{16.27}O_{62}$	-0.4	-	-	-	[75]
NENU-3/CC[d]	-0.5	5–560	45.11	0.55	[28]
S_2W_{18}-doped PEDOT (Voltammetric)		2000-10000	229.84	380	This work
S_2W_{18}-doped PEDOT (Chronoamperometric)	-0.1	100-2000	97.59	4	This work

[a]-Silver Nanoparticles, [b]-Carbon Paste Electrode, [c]-Polyaniline, [d]- Carbon Cloth

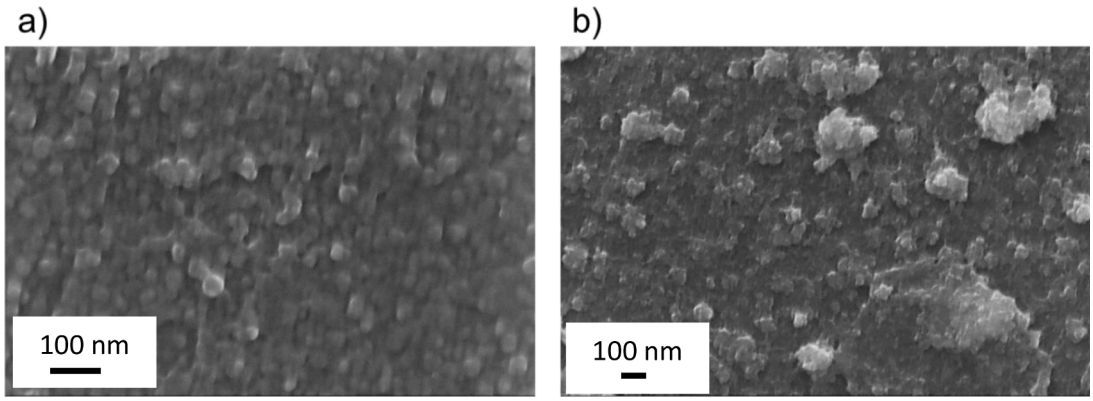

Fig. 12. FE-SEM micrographs of a) 2 mC and b) 10 mC S_2W_{18}-doped PEDOT films.

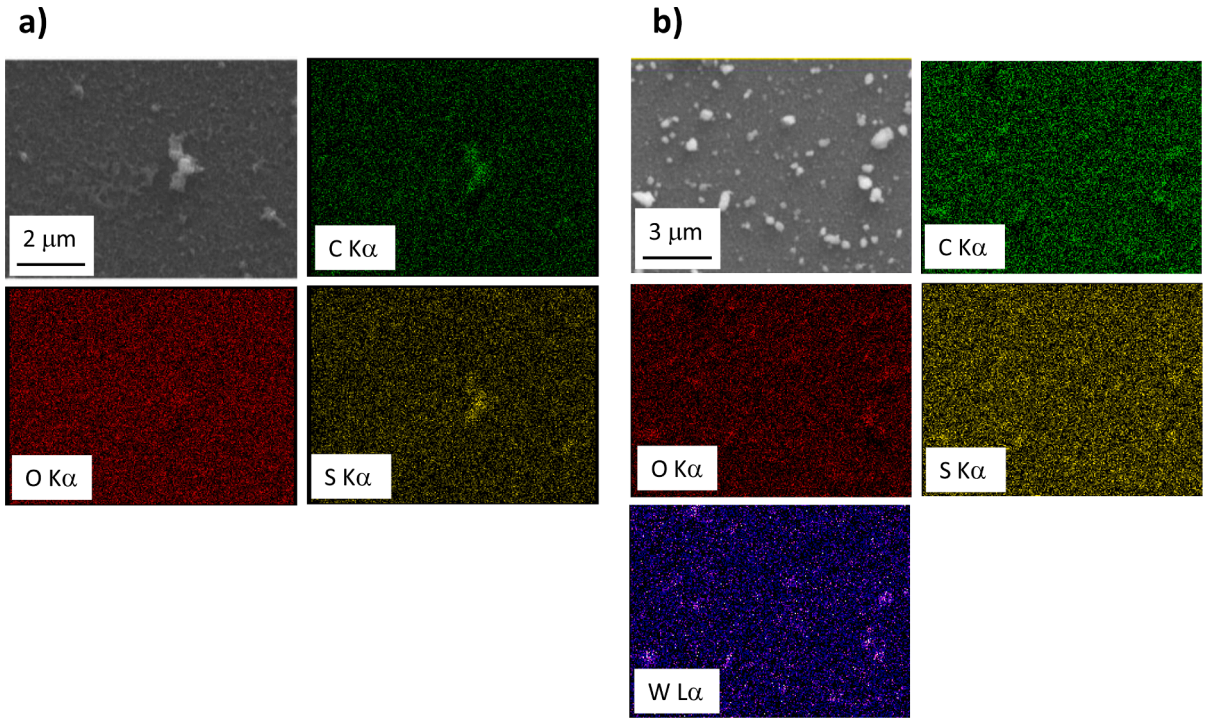

Fig. 13. EDXS elemental maps, recorded on the areas imaged in the corresponding FE-SEM micrographs, for a) PEDOT-only film; b) 2 mC S_2W_{18}-doped PEDOT film.

reported catalysts. As stated in the introduction section, the Well-Dawson type POM has been less studied than the Keggin type POM [28,32,33,72]. The bromate reduction potential of S_2W_{18}-doped PEDOT was very close to the reported reduction potential of PMo_{12}/PEDOT/AuNP/GC [33] and $[Ni_4(P_8W_{48}O_{184})(WO_2)]^{28-}$ POM+PPY film [25]. Aixiang Tian *et al* achieved an improved sensitivity towards the bromate ion by employing the carbon paste electrode made with $[(Cu_2(H_2bdpm)_2)[H_2P_2W_{18}O_{62}]_{0.5}]\cdot 2H_2O$ with an applied potential of + 0.4 V vs Ag/AgCl [34].

Polyaniline–POM [32] and NENU-3/CC [28] showed a linear range starting from 7.5 and 5 µmol L^{-1} respectively. It is noteworthy that the Polyaniline-POM and NENU-3/CC were found to have applied reduction potentials of -0.3 and -0.5 V, respectively. An inorganic-organic hybrid solid $(H_{6/5}bppy)^{5-}$ $[P_2W_{18}O_{62}]\cdot 4.5H_2O$ (bppy = 4-(5-(4-bromophenyl) pyridin-2-yl-)pyridine) was hydrothermally synthesised and employed as an electrochemical bromate sensor [73]. The twin-$H_{1.73}P_2As_{1.73}W_{16.27}O_{62}$ clusters contain a modified Dawson-type unit that was synthesised and utilised as a bromate sensor. Anderson-type Polyoxometalate-based metal-organic complexes [74] have also been investigated as an electrochemical catalyst for bromate detection in water. The S_2W_{18}-doped PEDOT displayed much-improved bromate reduction potential as compared to the reported literature. Moreover, the catalyst loading over the electrode surface was high in most of the referenced literature given in Table 4, compared to our S_2W_{18}-doped PEDOT-modified electrode.

3.6. Chemico-physical characterization

S_2W_{18}-doped PEDOT (2 mC and 10 mC) films were deposited on the surface of ITO-coated glass plates to investigate their morphology.. The plane view FE-SEM image of the S_2W_{18}-PEDOT (2 mC), displayed in Fig. 12a, showed a globular texture, with evenly distributed spherical grains characterized by a mean size of 26 nm. A similar globular nano-organization of PEDOT has already been reported in the literature [76–78]. In the case of sample S_2W_{18}-doped PEDOT (10 mC), the analyses highlighted the formation of bigger grains (mean size = 80 nm) deriving from the aggregation of smaller spherical ones (mean size = 20 nm; Fig. 12b).

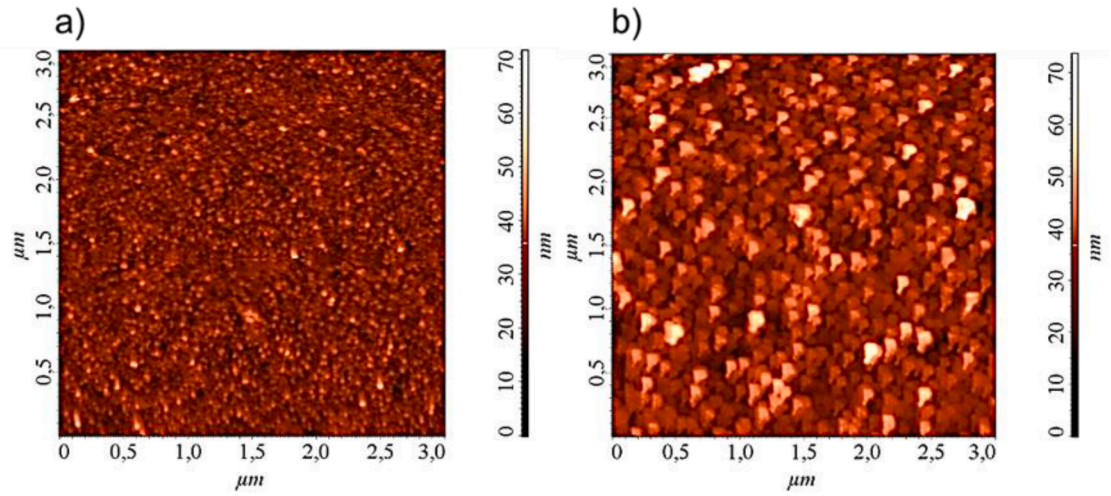

Fig. 14. Representative AFM topographical images of a) 2 mC and b) 10 mC S_2W_{18}-doped PEDOT film.

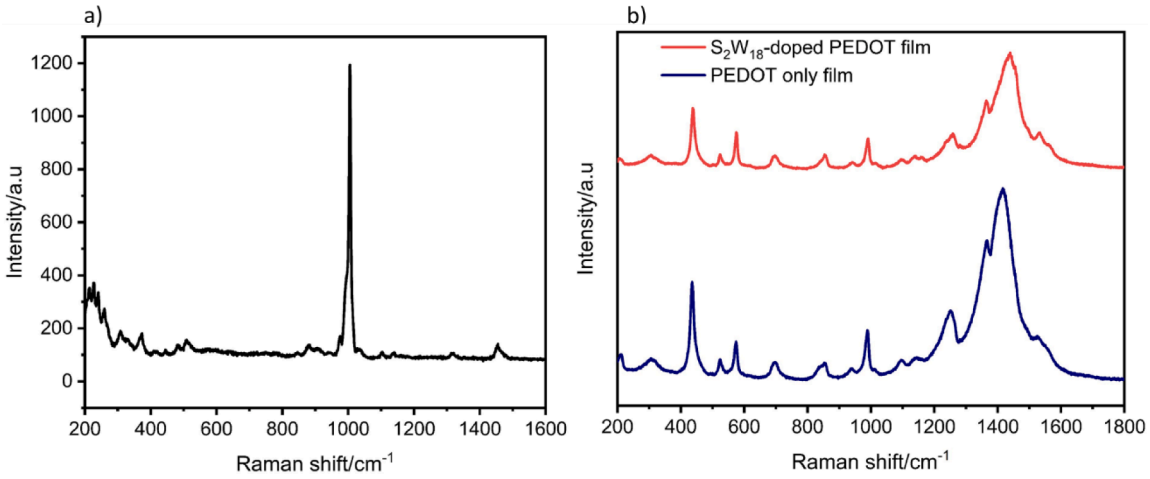

Fig. 15. Shows the Raman spectrum of a) S_2W_{18} powder and b) S_2W_{18}-doped PEDOT film (2 mC) and PEDOT-only film.

In-plane EDXS compositional mapping was performed on the S_2W_{18}-doped PEDOT and PEDOT-only films (Fig. 13a and b, respectively). As expected, the presence of C, O and S was observed for PEDOT-only film, whereas the presence of tungsten in S_2W_{18}-doped PEDOT confirmed the presence of S_2W_{18} moieties. The results obtained by maps registered in different regions pointed out to homogeneous material composition. Due to the significant polymer contribution, EDXS studies on the 10 mC film were unable to detect any clearly discernible W signal.

AFM topographical images were recorded for the 2 mC and 10 mC films and represented in Fig. 14a and b, respectively. The obtained results confirmed the globular sample topography, with an increase of RMS-roughness from 5 to 10 nm on passing from the 2 mC to the 10 mC sample. The increased roughness value of the latter, corresponding to a higher material loading, can be correlated to the formation of larger features, as confirmed by the above-discussed FE-SEM pictures.

3.7. Raman spectroscopy analysis

Raman spectroscopy analysis was carried out to further examine the nature of the interaction between S_2W_{18} and the PEDOT film. Using the method outlined in section 2.3, the film was created on the ITO-coated glass slide in order to record the Raman spectra. Fig. 15a and b show the Raman spectrum of S_2W_{18} powder, PEDOT film alone and S_2W_{18}-doped PEDOT respectively, on the ITO-coated glass slides. The Raman spectra of S_2W_{18} powder under excitation (785 nm) show several WO and SO stretching modes at 987 and 897 cm^{-1} and 1058 and 1131 cm^{-1}, respectively. These data were matched with the similar compounds reported in the previous literature [35,38,79]. In addition, OWO bending modes were observed at 597 and 520 cm^{-1} as we can see from Fig. 15a. The bands at 1322 and 1461 cm^{-1} were associated with the quaternary ammonium cation present in the POM structure. The vibrational modes of PEDOT are located at 1524 cm^{-1}, 1416 cm^{-1}, 1370 cm^{-1}, and 1250 cm^{-1}, and assigned to the $C_\alpha{=}C_\beta$ asymmetrical, $C_\alpha{=}C_\beta$ symmetrical, C_β-C_β stretching, and C_α-$C_{\alpha'}$ inter-ring stretching vibrations, respectively [80,81].

The Raman spectra of S_2W_{18}-doped PEDOT reveal that the majority of the peak is related to the PEDOT (Fig. 15b). Moreover, no significant peaks from the S_2W_{18} were observed in the spectrum, which could be attributed to the S_2W_{18} peaks being too weak and/or overlapping with the PEDOT peaks. The characteristic PEDOT band, which was previously at 1416 cm^{-1} in the S_2W_{18}-doped PEDOT film, has now moved to 1440 cm^{-1}. This is related to a higher doping level of PEDOT in the presence of POMs [82]. From the above evidence, a composite material was not formed; rather, S_2W_{18} was simply doped into the PEDOT film. The increased conjugation length of PEDOT chains in S_2W_{18}-doped PEDOT is indicated by the intensity ratio of the C-C to C-C stretching band for S_2W_{18}-doped PEDOT films being greater than that of PEDOT films [83, 84].

4. Conclusions

This work demonstrates the feasibility of the formation of the S_2W_{18}-doped PEDOT film on the glassy carbon electrode. The electrochemical behaviour of the hybrid film with various surface thicknesses was studied by cyclic voltammetry and electrochemical impedance spectroscopy. Three couples of redox peaks were observed in cyclic voltammograms of the S_2W_{18}-doped PEDOT film in pH 2 buffer solution, which were associated with two-electron transferred processes of tungsten coupled with proton and the polymer background. The surface-confined nature of the hybrid films is kept up to 100 mV/s. Voltammetric behaviour of the S_2W_{18}-doped PEDOT film is proton dependent, which peaks associated with two electron transfers that occurred at pH 2 split into several peaks corresponding to one electron transferred process. The electrical parameters, charge transfer resistance (R_{ct}), solution resistance (R_i), CPE, and the current density (i_o) for these films (in oxidized, partially reduced, and reduced states) were calculated and analyzed from EIS measurements of the S_2W_{18}-doped PEDOT film.

Electrocatalytic activity for the bromate reduction was observed for the S_2W_{18}-doped PEDOT monitored using both voltammetric and amperometric techniques. In the voltammetric mode, the linear range was observed from 2000 μmol L^{-1} to 10 000 μmol L^{-1} with a sensitivity of about 229 μA/mmol $L^{-1}cm^2$. In the chronoamperometric mode, the linear range is 100 μmol L^{-1} to 2000 μmol L^{-1} with a sensitivity of 97.59 μA/mmol $L^{-1}cm^2$ was observed. The LOD was calculated as 4 μmol L^{-1} and 380 μmol L^{-1} for amperometric and voltammetric techniques respectively. The S_2W_{18}-doped PEDOT-modified electrodes reveal high sensitivity towards the bromate system without any interference from the other analytes present in the real sample.

Declaration of Competing Interest

The authors declare that they have no known competing financial interests or personal relationships that could have appeared to influence the work reported in this paper.

Data availability

Data will be made available on request.

Acknowledgment

The authors acknowledge the Dundalk Institute of Technology for funding this project and Padova University and Dublin City University for surface analysis support.

This work was supported by the JSPS Core-to-Core Collaboration in Advanced Research Network, International Network on Polyoxometalate Science for Advanced Functional Energy Materials, the Cooperative Research Program of "Network Joint Research Center for Materials and Devices, Takahashi Industrial and Economic Research Foundation, CNR (Progetti di Ricerca @CNR – avviso 2020 - ASSIST), Padova University (P-DiSC#04-BIRD2020-UNIPD EUREKA), and INSTM Consortium (INSTM21PDBARMAC – ATENA).

Credit author statement

Timothy McCormac, interpretation of electrochemical results

Davide Barreca and Chiara Maccato, performance and interpretation of surface based techniques

Indherjith Sakthinathan, performance of electrochemical techniques

Naoki Yamasaki and Tadaharu Ueda, POM synthesis and characterisation

References

[1] S. Herrmann, C. Ritchie, C. Streb, Polyoxometalate – conductive polymer composites for energy conversion, energy storage and nanostructured sensors, Dalt. Trans. 44 (2015) 7092–7104, https://doi.org/10.1039/C4DT03763D.

[2] Y. Cao, Q. Chen, C. Shen, L. He, Polyoxometalate-based catalysts for CO2 conversion, Molecules 24 (2019), https://doi.org/10.3390/molecules24112069.

[3] M. Blasco-Ahicart, J. Soriano-Lopez, J.J. Carbo, J.M. Poblet, J.R. Galan-Mascaros, Polyoxometalate electrocatalysts based on earthabundant metals for efficient water oxidation in acidic media, Nat. Chem. 10 (2018) 24–30, https://doi.org/10.1038/NCHEM.2874.

[4] T. Ueda, Electrochemistry of polyoxometalates: From fundamental aspects to applications, ChemElectroChem 5 (2018) 823–838, https://doi.org/10.1002/celc.201701170.

[5] C. Yuan, S. Guo, S. Wang, L. Liu, W. Chen, E. Wang, Electropolymerization polyoxometalate (POM)-doped pedot film electrodes with mastoid microstructure and its application in dye-sensitized solar cells (DSSCs), Ind. Eng. Chem. Res. 52 (2013) 6694–6703, https://doi.org/10.1021/ie302845z.

[6] R. Sivakumar, J. Thomas, M. Yoon, Polyoxometalate-based molecular/nano composites: advances in environmental remediation by photocatalysis and biomimetic approaches to solar energy conversion, J. Photochem. Photobiol. C Photochem. Rev. 13 (2012) 277–298, https://doi.org/10.1016/j.jphotochemrev.2012.08.001.

[7] A. Dolbecq, P. Mialane, B. Keita, L. Nadjo, Polyoxometalate-based materials for efficient solar and visible light harvesting: application to the photocatalytic degradation of azo dyes, J. Mater. Chem. 22 (2012) 24509–24521, https://doi.org/10.1039/c2jm33246a.

[8] S. Imar, M. Yaqub, C. Maccato, C. Dickinson, F. Laffir, M. Vagin, T. McCormac, Nitrate and nitrite electrocatalytic reduction at layer-by-layer films composed of dawson-type heteropolyanions mono-substituted with transitional metal ions and silver nanoparticles, Electrochim. Acta. 184 (2015) 323–330, https://doi.org/10.1016/j.electacta.2015.10.082.

[9] T. Ueda, Polyoxometalates in analytical sciences, Anal. Sci 37 (2021) 107–118, https://doi.org/10.2116/ANALSCI.20SAR17.

[10] X. Chen, J. Pan, J. Fu, X. Zhu, C. Zhang, L. Zhou, Y. Wang, Z. Lv, Y. Zhou, S.T. Han, Polyoxometalates-modulated reduced graphene oxide flash memory with ambipolar trapping as bidirectional artificial synapse, Adv. Electron. Mater. 4 (2018) 1–9, https://doi.org/10.1002/aelm.201800444.

[11] X. Chen, X. Zhu, S.R. Zhang, J. Pan, P. Huang, C. Zhang, G. Ding, Y. Zhou, K. Zhou, V.A.L. Roy, S.T. Han, Controlled nonvolatile transition in polyoxometalates-graphene oxide hybrid memristive devices, Adv. Mater. Technol. 4 (2019) 1–9, https://doi.org/10.1002/admt.201800551.

[12] L. Vilà-Nadal, S.G. Mitchell, S. Markov, C. Busche, V. Georgiev, A. Asenov, L. Cronin, Towards polyoxometalate-cluster-based nano-electronics, Chem. - A Eur. J. 19 (2013) 16502–16511, https://doi.org/10.1002/chem.201301631.

[13] J.J. Walsh, A.M. Bond, R.J. Forster, T.E. Keyes, Hybrid polyoxometalate materials for photo(electro-) chemical applications, Coord. Chem. Rev. 306 (2016) 217–234, https://doi.org/10.1016/j.ccr.2015.06.016.

[14] M.H. Yang, D.S. Kim, J.H. Yoon, S.B. Hong, S.W. Jeong, D.E. Yoo, T.J. Lee, S.J. Lee, K.G. Lee, B.G. Choi, Nanopillar films with polyoxometalate-doped polyaniline for electrochemical detection of hydrogen peroxide, Analyst 141 (2016) 1319–1324, https://doi.org/10.1039/c5an02134k.

[15] A.F. Murphy, T. McCormac, Surface immobilisation of transition metal substituted Krebs type polyoxometalates, [X2W20M2O70(H2O)6]n- (X = Bi or Sb, M = Co2+ or Cu2+), by the layer by layer technique, Electrochim. Acta. 56 (2011) 10751–10761, https://doi.org/10.1016/j.electacta.2011.04.089.

[16] R. Naseer, S.S. Mal, M. Ibrahim, U. Kortz, G. Armstrong, F. Laffir, C. Dickinson, M. Vagin, T. McCormac, Redox, surface and electrocatalytic properties of layer-by-layer films based upon Fe(III)-substituted crown polyoxometalate [P8W48O184Fe16(OH)28(H2O)4]20, Electrochim. Acta. 134 (2014) 450–458, https://doi.org/10.1016/j.electacta.2014.03.099.

[17] K. Dalla Francesca, S. Lenfant, M. Laurans, F. Volatron, G. Izzet, V. Humblot, C. Methivier, D. Guerin, A. Proust, D. Vuillaume, Charge transport through redox active [H7P8W48O184]33- polyoxometalates self-assembled onto gold surfaces and gold nanodots, Nanoscale 11 (2019) 1863–1878, https://doi.org/10.1039/c8nr09377f.

[18] Y.L. Zhong, W. Ng, J.X. Yang, K.P. Loh, Electrostatically self-assembled polyoxometalates on molecular-dye- functionalized diamond, J. Am. Chem. Soc. 131 (2009) 18293–18298, https://doi.org/10.1021/ja908131t.

[19] Y.Y. Bao, L.H. Bi, L.X. Wu, S.S. Mal, U. Kortz, Preparation and characterization of Langmuir-Blodgett films of wheel-shaped Cu-20 tungstophosphate and DODA by two different strategies, Langmuir 25 (2009) 13000–13006, https://doi.org/10.1021/la901854e.

[20] M. Clemente-León, E. Coronado, C.J. Gómez-García, C. Mingotaud, S. Ravaine, G. Romualdo-Torres, P. Delhaès, Polyoxometalate monolayers in Langmuir-Blodgett films, Chem. - A Eur. J. 11 (2005) 3979–3987. https://doi.org/10.1002/chem.200401063.

[21] W. Qi, H. Li, L. Wu, A novel, luminescent, silica-sol-gel hybrid based on surfactant-encapsulated polyoxometalates, Adv. Mater. 19 (2007) 1983–1987, https://doi.org/10.1002/adma.200602430.

[22] J. Wang, F. Liu, L. Fu, H. Zhang, Luminescence properties of rare earth-polyoxometalate thin film deposited by sol-gel process, Mater. Lett. 56 (2002) 300–304, https://doi.org/10.1016/S0167-577X(02)00459-7.

[23] S.M. Wang, L. Liu, W.L. Chen, Z.M. Zhang, Z.M. Su, E.B. Wang, A new electrodeposition approach for preparing polyoxometalates-based electrochromic

smart windows, J. Mater. Chem. A. 1 (2013) 216–220, https://doi.org/10.1039/c2ta00486k.
[24] Y.Z. Liu, W. Yao, H.M. Gan, C.Y. Sun, Z.M. Su, X.L. Wang, Polyoxometalates-based metal–organic frameworks made by electrodeposition and carbonization methods as cathodes and anodes for asymmetric supercapacitors, Chem. - A Eur. J. 25 (2019) 16617–16624, https://doi.org/10.1002/chem.201903664.
[25] B. Ali, F. Laffir, L. Kailas, G. Armstrong, L. Kailas, R. O'Connell, T. McCormac, Electrochemical characterisation of niii-crown-type polyoxometalate-doped polypyrrole films for the catalytic reduction of bromate in water, Eur. J. Inorg. Chem. 2019 (2019) 394–401, https://doi.org/10.1002/ejic.201801106.
[26] R. Naseer, B. Ali, F. Laffir, L. Kailas, C. Dickinson, G. Armstrong, T. McCormac, Transition metal-substituted krebs-type polyoxometalate-doped PEDOT films, Langmuir 35 (2019) 11007–11015, https://doi.org/10.1021/acs.langmuir.8b03785.
[27] D.M. Fernandes, C.M.A. Brett, A.M.V. Cavaleiro, Preparation and electrochemical properties of modified electrodes with Keggin-type silicotungstates and PEDOT, J. Electroanal. Chem. 660 (2011) 50–56, https://doi.org/10.1016/j.jelechem.2011.06.004.
[28] Y. Zhang, Y. Zhang, L. Li, J. Chen, P. Li, W. Huang, One-step in situ growth of high-density POMOFs films on carbon cloth for the electrochemical detection of bromate, J. Electroanal. Chem. 861 (2020), 113939, https://doi.org/10.1016/j.jelechem.2020.113939.
[29] Y. Ji, L. Huang, J. Hu, C. Streb, Y.F. Song, Polyoxometalate-functionalized nanocarbon materials for energy conversion, energy storage and sensor systems, Energy Environ. Sci. 8 (2015) 776–789, https://doi.org/10.1039/c4ee03749a.
[30] M.R. Majidi, S. Ghaderi, K. Asadpour-Zeynali, H. Dastangoo, Electrochemical determination of bromate in different types of flour and bread by a sensitive amperometric sensor based on palladium nanoparticles/graphene oxide nanosheets, Food Anal. Methods. 8 (2015) 2011–2019, https://doi.org/10.1007/s12161-014-0065-7.
[31] R. Butler, A. Godley, L. Lytton, E. Cartmell, Bromate environmental contamination: review of impact and possible treatment, Crit. Rev. Environ. Sci. Technol. 35 (2005) 193–217, https://doi.org/10.1080/10643380590917888.
[32] G.G. Papagianni, D.V. Stergiou, G.S. Armatas, M.G. Kanatzidis, M.I. Prodromidis, Synthesis, characterization and performance of polyaniline-polyoxometalates (XM12, X = P, Si and M = Mo, W) composites as electrocatalysts of bromates, Sensors Actuators, B Chem 173 (2012) 346–353, https://doi.org/10.1016/j.snb.2012.07.020.
[33] S.S. Hassan, Y. Liu, A.R.Solangi Sirajuddin, A.M. Bond, J. Zhang, Phosphomolybdate-doped-poly(3,4-ethylenedioxythiophene) coated gold nanoparticles: Synthesis, characterization and electrocatalytic reduction of bromate, Anal. Chim. Acta. 803 (2013) 41–46, https://doi.org/10.1016/j.aca.2013.04.036.
[34] A. Tian, M. Yang, H. Ni, N. Sun, Y. Yang, Y. Fu, J. Ying, Use of symmetrical and pendant pyrazole derivatives for the construction of two polyoxometalate-based complexes as electrochemical sensors, Transit. Met. Chem. 43 (2018) 621–633, https://doi.org/10.1007/s11243-018-0250-4.
[35] S. Himeno, H. Tatewaki, M. Hashimoto, Synthesis, structure, and [S2W18O62]4− complex characterization of an α -Dawson-type, Bull. Chem. Soc. Japan. 74 (2001) 1623–1628.
[36] N.K. Sarangi, A. Prabhakaran, T.E. Keyes, Multimodal investigation into the interaction of quinacrine with microcavity-supported lipid bilayers, Langmuir (2022), https://doi.org/10.1021/acs.langmuir.2c00524.
[37] Gianluca Bernardini, A.G. Wedd, C. Zhao, A.M. Bond, Electrochemical probing of the photoreduction of molybdenum and tungsten Dawson-type polyoxometalates in molecular and ionic liquid media using water as an electron donor, Dalt. Trans. 41 (2012) 9944–9954.
[38] T. Ueda, M. Ohnishi, M. Shiro, J. Nambu, T. Yonemura, J.F. Boas, A.M. Bond, Synthesis and characterization of novel Wells-Dawson-type mono vanadium(V)-substituted tungsto-polyoxometalate isomers: 1- and 4-[S 2 VW 17 O 62] 5-, Inorg. Chem. 53 (2014) 4891–4898, https://doi.org/10.1021/ic402994q.
[39] N. Elgrishi, K.J. Rountree, B.D. McCarthy, E.S. Rountree, T.T. Eisenhart, J. L. Dempsey, A practical beginner's guide to cyclic voltammetry, J. Chem. Educ. 95 (2018) 197–206, https://doi.org/10.1021/acs.jchemed.7b00361.
[40] M.A. Rahman, J. Li, S.X. Guo, G. Kennedy, T. Ueda, A.M. Bond, J. Zhang, Modelling limitations encountered in the thermodynamic and electrode kinetic parameterization of the α-[S2W18O62]4−/5−/6− processes at glassy carbon and metal electrodes, J. Electroanal. Chem. (2020), 113786, https://doi.org/10.1016/j.jelechem.2019.113786.
[41] W. Lövenich, PEDOT-properties and applications, Polym. Sci. - Ser. C. 56 (2014) 135–143, https://doi.org/10.1134/S1811238214010068.
[42] P. Kumar, Z. Yi, S. Zhang, A. Sekar, F. Soavi, F. Cicoira, Effect of channel thickness, electrolyte ions, and dissolved oxygen on the performance of organic electrochemical transistors, Appl. Phys. Lett. 107 (2015), https://doi.org/10.1063/1.4927595, 053303 (1–5).
[43] B. Ali, I. Sakthinathan, D. Barreca, C. Maccato, J. Goura, U. Kortz, T. McCormac, Tetra-MnIII-containing 30-Tungsto-4-phosphate, [MnIII4(H2O)2(P2W15O56)2] 12-: Entrapped PEDOT films, surface analysis and electrochemical study Symmetrical [NaNi3(H2O)2(P2W15O56)2]17- and [CoNi3(H2O)2(P2W15O56)2] 16- Anions, Thin Solid Films 766 (2023), 139610, https://doi.org/10.1002/chin.201004021.
[44] D. Jacob, P.A. Mini, A. Balakrishnan, S.V. Nair, K.R.V. Subramanian, Electrochemical behaviour of graphene-poly (3,4-ethylenedioxythiophene) (PEDOT) composite electrodes for supercapacitor applications, Bull. Mater. Sci. 37 (2014) 61–69, https://doi.org/10.1007/s12034-013-0610-9.
[45] S.J. Higgins, K.V. Lovell, R.M.G. Rajapakse, N.M. Walsby, Grafting and electrochemical characterisation of poly-(3,4- ethylenedioxythiophene) films, on Nafion and on radiation-grafted polystyrenesulfonate-polyvinylidene fluoride composite surfaces, J. Mater. Chem. 13 (2003) 2485–2489, https://doi.org/10.1039/b303424k.
[46] H. Randriamahazaka, C. Plesse, D. Teyssié, C. Chevrot, Electrochemical behaviour of poly(3,4-ethylenedioxythiophene) in a room-temperature ionic liquid, Electrochem. Commun. 5 (2003) 613–617, https://doi.org/10.1016/S1388-2481(03)00142-5.
[47] M. Skompska, Alternative explanation of asymmetry in cyclic voltammograms for redox reaction of poly(3-methylthiophene) films in acetonitrile solutions, Electrochim. Acta. 44 (1998) 357–362, https://doi.org/10.1016/S0013-4686(98)00058-9.
[48] M. Skompska, A. Jackson, A.R. Hillman, Evolution from gravimetric to viscoelastic response of poly(3-methylthiophene)-loaded acoustic wave resonators, Phys. Chem. Chem. Phys. 2 (2000) 4748–4757, https://doi.org/10.1039/b004807k.
[49] A. Robert Hillman, S.J. Daisley, S. Bruckenstein, Solvent effects on the electrochemical p-doping of PEDOT, Phys. Chem. Chem. Phys. 9 (2007) 2379–2388, https://doi.org/10.1039/b618786b.
[50] J. Scotto, E. Piccinini, C. von Bilderling, L.L. Coria-Oriundo, F. Battaglini, W. Knoll, W.A. Marmisolle, O. Azzaroni, Flexible conducting platforms based on PEDOT and graphite nanosheets for electrochemical biosensing applications, Appl. Surf. Sci. 525 (2020), 146440, https://doi.org/10.1016/j.apsusc.2020.146440.
[51] A. Yaqub, M. Vagin, J.J. Walsh, F. Laffir, I. Sakthinathan, T. McCormac, M. Yaqub, Organic-inorganic hybrid films of the sulfate Dawson polyoxometalate, [S2W18O62]4- and polypyrrole for iodate electrocatalysis, ACS Omega 7 (2022) 43381–43389, https://doi.org/10.1021/acsomega.2c01287.
[52] M. Yaqub, J. Walsh, F. Laffir, P. Olstoorn, L. Kailas, R. Forster, T.E. Keyes, M. Vagin, T. McCormac, Polypyrrole entrapped 18-molybdodisulphate anion for the detection of hydrogen peroxide, Electrochim. Acta. 287 (2018) 78–86, https://doi.org/10.1016/j.electacta.2018.08.053.
[53] F. Branzoi, V. Branzoi, The electrochemical behaviour of PEDOT film electrosynthesized in presence of some dopants, Open J. Org. Polym. Mater. 05 (2015) 89–102, https://doi.org/10.4236/ojopm.2015.54010.
[54] N. Anwar, M. Vagin, F. Laffir, G. Armstrong, C. Dickinson, T. McCormac, Transition metal ion-substituted polyoxometalates entrapped in polypyrrole as an electrochemical sensor for hydrogen peroxide, Analyst 137 (2012) 624–630, https://doi.org/10.1039/c1an15665a.
[55] Y. Tanaka, T. Hasegawa, T. Shimamura, H. Ukeda, Potentiometric evaluation of antioxidant capacity using polyoxometalate- immobilized electrodes, J. Electroanal. Chem. 828 (2018) 102–107, https://doi.org/10.1016/j.jelechem.2018.09.024.
[56] T. Ueda, K. Kodani, H. Ota, M. Shiro, S. Guo, J.F. Boas, A.M. Bond, Voltammetric and spectroscopic studies of α- and β-[PW12O40]3− polyoxometalates in neutral and acidic media: structural characterization as their [(n-Bu4N)3][PW12O40] salts, Inorg. Chem 56 (2017) 3990–4001, https://doi.org/10.1021/acs.inorgchem.6b03046.
[57] T. Ueda, J. Nambu, J. Lu, S. Guo, Q. Li, J.F. Boas, L.L. Martin, A.M. Bond, Structurally characterised vanadium(V)-substituted Keggin-type heteropolysulfates [SVM11O40]3− (M = Mo, W): voltammetric and spectroscopic studies related to the V(V)/V(IV) redox couple, Dalt. Trans. 43 (2014) 5462–5473, https://doi.org/10.1039/c3dt53161a.
[58] J. Nambu, T. Ueda, S. Guo, F. Boas, A.M. Bond, Detailed voltammetric and EPR study of protonation reactions accompanying the one-electron reduction of Keggin-type polyoxometalates, [XVVM11O40]4- (X = P, As ; M = Mo, W) in acetonitrile, Dalt. Trans. 39 (2010) 7364–7373, https://doi.org/10.1039/c003248d.
[59] T. Ueda, M. Ohnishi, D. Kawamoto, S.X. Guo, J.F. Boas, A.M. Bond, Voltammetric behavior of 1- and 4-[S2VW17O62]5- in acidified acetonitrile, Dalt. Trans. 44 (2015) 11660–11668, https://doi.org/10.1039/c5dt01530h.
[60] R.N. Vyas, B. Wang, Electrochemical analysis of conducting polymer thin films, Int. J. Mol. Sci. 11 (2010) 1956–1972, https://doi.org/10.3390/ijms11041956.
[61] J.F. Rubinson, Y.P. Kayinamura, Charge transport in conducting polymers: Insights from impedance spectroscopy, Chem. Soc. Rev. 38 (2009) 3339–3347, https://doi.org/10.1039/b904083h.
[62] D. Zhang, H. Ma, Y. Chen, H. Pang, Y. Yu, Amperometric detection of nitrite based on Dawson-type vanodotungstophosphate and carbon nanotubes, Anal. Chim. Acta. 792 (2013) 35–44, https://doi.org/10.1016/j.aca.2013.07.010.
[63] D.M. Fernandes, C.M.A. Brett, A.M.V. Cavaleiro, Layer-by-layer self-assembly and electrocatalytic properties of poly(ethylenimine)-silicotungstate multilayer composite films, J. Solid State Electrochem. 15 (2011) 811–819, https://doi.org/10.1007/s10008-010-1154-1.
[64] M. De Keersmaecker, J.R. Reynolds, Simple interface modification of electroactive polymer film electrodes, ACS Appl. Mater. Interfaces. 11 (2019) 47131–47142, https://doi.org/10.1021/acsami.9b16045.
[65] L.F. Marchesi, S.C. Jacumasso, R.C. Quintanilha, H. Winnischofer, M. Vidotti, The electrochemical impedance spectroscopy behavior of poly(aniline) nanocomposite electrodes modified by Layer-by-Layer deposition, Electrochim. Acta. 174 (2015) 864–870, https://doi.org/10.1016/j.electacta.2015.05.077.
[66] C.T. Zhu, Y. Yang, F.Y. Lin, Y. Luo, S.P. Ma, L. Zhu, X.Y. Guo, Electrodeposited transparent PEDOT for inverted perovskite solar cells: improved charge transport and catalytic performances, Rare Met 40 (2021) 2402–2414, https://doi.org/10.1007/s12598-020-01641-9.
[67] C.A. Downes, A.J. Clough, K. Chen, J.W. Yoo, S.C. Marinescu, Evaluation of the H2 evolving activity of benzenehexathiolate coordination frameworks and the effect of film thickness on H2 production, ACS Appl. Mater. Interfaces. 10 (2018) 1719–1727, https://doi.org/10.1021/acsami.7b15969.

[68] M. Zhong, P. Yang, B. Hou, M. Xia, J. Wang, Tuning the catalytic performance of Fischer-Tropsch synthesis by regulating the Al2O3-layer over Co/Al2O3/Al catalysts, Fuel 314 (2022), 122136, https://doi.org/10.1016/j.fuel.2021.122136.
[69] R. Mao, X. Zhao, H. Lan, H. Liu, J. Qu, Graphene-modified Pd/C cathode and Pd/GAC particles for enhanced electrocatalytic removal of bromate in a continuous three-dimensional electrochemical reactor, Water Res. 77 (2015) 1–12, https://doi.org/10.1016/j.watres.2015.03.002.
[70] Z. Lu, Q. Yang, T. Hu, J. Wang, W. Tang, FeIIAlIII layered double hydroxide modified carbon-felt cathode for efficient electrochemical reduction of bromate, Chem. Eng. J. 446 (2022), 137356, https://doi.org/10.1016/j.cej.2022.137356.
[71] Q. Li, Q. Zhang, L. Ding, D. Zhou, H. Cui, Z. Wei, J. Zhai, Synthesis of silver/multi-walled carbon nanotubes composite and its application for electrocatalytic reduction of bromate, Chem. Eng. J. 217 (2013) 28–33, https://doi.org/10.1016/j.cej.2012.12.005.
[72] M. Skunik, P.J. Kulesza, Phosphomolybdate-modified multi-walled carbon nanotubes as effective mediating systems for electrocatalytic reduction of bromate, Anal. Chim. Acta. 631 (2009) 153–160, https://doi.org/10.1016/j.aca.2008.10.031.
[73] A. Tian, Z. Han, J. Peng, J. Zhai, Y. Zhao, Inorganic-organic microporous solid of Wells-Dawson type polyoxometalate: Synthesis, characterization, and electrochemical properties, Zeitschrift Fur Anorg. Und Allg. Chemie. 633 (2007) 495–503, https://doi.org/10.1002/zaac.200600320.
[74] X. Wang, J. Sun, H. Lin, Z. Chang, X. Wang, G. Liu, A series of Anderson-type polyoxometalate-based metal–organic complexes: pH-dependent electrochemical behaviours and as electrocatalysts and photocatalysts, Dalt. Trans. 45 (2016) 12465–12478, https://doi.org/10.1039/b000000x.
[75] B. Lu, S. Li, X. Zhang, D. Zhang, L. Fan, E. Yan, Y. Zhang, L. Yu, A novel polyoxometalate-based metal-organic nanotube framework templated by twin-Dawson clusters: Synthesis, structure and bifunctional electrocatalytic properties, New J. Chem. 43 (2019) 15804–15810, https://doi.org/10.1039/c9nj02004g.
[76] B.M. Hryniewicz, M. Vidotti, PEDOT nanotubes electrochemically synthesized on flexible substrates: enhancement of supercapacitive and electrocatalytic properties, ACS Appl. Nano Mater. 1 (2018) 3913–3924, https://doi.org/10.1021/acsanm.8b00694.
[77] A. Sulowska, A. Fiszka, K. Cysewska, K. Nikiforow, G. Trykowski, A. Zieli, The effect of PEDOT morphology on hexavalent chromium reduction over 2D TiO 2 /PEDOT photocatalyst under UV – vis light, Mater. Chem. Phys. 299 (2023), 127430, https://doi.org/10.1016/j.matchemphys.2023.127430.
[78] S. Patra, N. Munichandraiah, Supercapacitor studies of electrochemically deposited PEDOT on stainless steel substrate, J. Appl. Polym. Sci. 106 (2007) 1160–1171, https://doi.org/10.1002/app.
[79] M.K. Seery, L. Guerin, R.J. Forster, E. Gicquel, V. Hultgren, A.M. Bond, A.G. Wedd, T.E. Keyes, Photophysics of ion clusters formed between [Ru(bpy)3]2+ and the polyoxotungstate anion [S2W18O62]4-, J. Phys. Chem. A. 108 (2004) 7399–7405, https://doi.org/10.1021/jp0482464.
[80] Q. Zhao, R. Jamal, L. Zhang, M. Wang, T. Abdiryim, The structure and properties of PEDOT synthesized by template-free solution method, Nanoscale Res. Lett. 9 (2014) 557, https://doi.org/10.1186/1556-276X-9-557, 1–9.
[81] S.H. Chang, C.-H. Chiang, F.-S. Kao, C.-L. Tien, C.-G. Wu, Unraveling the enhanced electrical conductivity of PEDOT : PSS thin films for unraveling the enhanced electrical conductivity of PEDOT : PSS thin films for ITO-free organic photovoltaics, IEEE Photonics J 6 (2014), https://doi.org/10.1109/JPHOT.2014.2331254, 8400307 (1–7).
[82] S. Sakamoto, M. Okumura, Z. Zhao, Y. Furukawa, Raman spectral changes of PEDOT-PSS in polymer light-emitting diodes upon operation, Chem. Phys. Lett. 412 (2005) 395–398, https://doi.org/10.1016/j.cplett.2005.07.040.
[83] B.P. Suma, P. Shivappa, S. Kumar, P. Malingappa, A new polyoxometalate /rGO / Pani composite modified electrode for electrochemical sensing of nitrite and its application to food and environmental samples, Mater. Chem. Phys. 229 (2019) 269–278, https://doi.org/10.1016/j.matchemphys.2019.02.087.
[84] M. Yang, S.B. Hong, J.H. Yoon, D.S. Kim, S.W. Jeong, D.E. Yoo, T.J. Lee, K.G. Lee, S.J. Lee, B.G. Choi, Fabrication of flexible, redoxable, and conductive nanopillar arrays with enhanced electrochemical performance, ACS Appl. Mater. Interfaces. 8 (2016) 22220–22226, https://doi.org/10.1021/acsami.6b06579.